Short Timescale Variability in Symbiotics: A Photometric Study

Louis Gregg

July 31, 2014

Abstract

A photometric study of rapid timescale variability in the symbiotic system EG And was carried out at B, V and R_C passbands, using data obtained at the Monck Observatory on 2013.11.12.
The presence of a variability could not be conclusively determined due to the small size of the data sets obtained. The limits of sensitivity to aperiodic variability were determined for the Monck Observatory.
Photometric data obtained with the KAIT telescope between 2001.06.20 and 2005.01.23 was used to form phased differential magnitude lightcurves for EG And. Differential photometry data obtained at the Monck was plotted over this.

Acknowledgements

I obtained magnitude data for EG And from the SIMBAD database. Brian Espey provided me with magnitude data from the Hipparcos satellite and the KAIT telescope. He also provided image sets obtained at the Monck and Imbusch observatories. Martin Topinka of UCD provided us with access to the Watcher telescope in South Africa. Ray Butler of NUI Galway provided me with technical information concerning the Imbusch Observatory's telescope.
Brian Espey and Joe McCauley supervised me in preparation for, and execution of, observation sessions at the Monck Observatory. Joe McCauley provided me with technical advice and documentation regarding the telescope's operation and image processing. Brian Espey gave notes on a draft of this report. I am grateful for the information, advice and encouragement offered by all parties.

Contents

Chapter 1

Introduction

The photometric study of symbiotic binary systems (SS) has the potential to yield a great deal of information about mass transfer processes occurring within these systems. The aim of this project was to identify periodic variability or aperiodic ”flickering” variability of the order of seconds to minutes, and to attribute this variability to processes occurring on the surfaces of the hot and cool components. An influential study for this project was Sokoloski et al. (2001). In this study, a number of SS were observed; limits were placed on the magnitude of flickering for a number of systems and periodic variability was also sought out.

Many statistical techniques used by Sokoloski et al. (2001) in the detection of aperiodic variability were adopted in our search for variability of similar timescales.

However, the small amount of data prevented any useful implementation of Fourier analysis techniques to identify periodic behaviour for this project.

The sensitivity of our analysis to detection of low-amplitude variations was dependent on the signal to noise ratio (SNR) obtained for the stars in the field. Much of the pre-processing techniques outlined in chapter 3.2 and analysis in chapter 4 were implemented to minimise noise and uncertainty in our final lightcurves.

For the data acquired at the Monck Observatory, a weighted-mean differential-ensemble photometry analysis was implemented to minimise uncertainty in the lightcurves produced. This was carried out using various combinations of the comparison stars available in order to obtain a curve for which the expected error was minimised.

Differential photometry with a single comparison star and a check star was also carried out.

Data from the KAIT telescope, California was used to form part of an orbital lightcurve for the target of the project, EG And.

Chapter 2

Theory and Background

2.1 Symbiotic Binary Systems

SS consist of a white dwarf (WD) (or occasionally, a neutron star), and a red giant (RG) orbiting a common centre of mass at a separation of several AU. These systems typically have an orbital period of the order of several years. Many SS have been observed to undergo outburst but the cause(s) of outburst remain uncertain. Indeed, many SS were first noticed by astronomers due to the system undergoing outburst.

Features often seen in typical symbiotic spectra are the absorption features of a late-type giant star, HI emission lines and HeI emission lines. These features are accompanied by either additional bright lines of ions with an ionisation potential of at least 20eV or, if in outburst, an A or F-type continuum with additional absorption lines from H I , He I, and singly ionized metals Kenyon (1986). SS are also considered to be a potential progenitor channel to type Ia supernovae.

Mass transfer in SS can take the form of two distinct types.The first type, Roche-lobe overflow, occurs when the atmosphere of the giant expands beyond the star's region of gravitational influence. When this occurs, mass is transferred onto the hot component through the inner Lagrangian point of the system.

The second mass transfer channel is accretion by the hot component of the RG's stellar wind, or if present, the surrounding nebula. Mass transfer rates in such a process are considered to be of the order of $10^{-8} M_{\odot} year^{-1}$. This process could be facilitated through disk accretion onto the hot component, or magnetic accretion onto the magnetic poles of the hot component. Wind accretion is considered to be a potential cause of flickering variability due to its sporadic nature.

2.2 EG Andromadae

The primary target in this study was the well studied system EG Andromadae (EG And, HIP 3494). EG And is a SS consisting of a WD or sub-WD and a M3III type giant. The orbital period of the system was calculated to be 482.2 days by Skopal et al. (1991). This value was further refined by Fekel et al. (2000), who obtained an orbital period of 482.57 ± 0.53, as calculated from four different sets of radial velocities, including those obtained in Skopal et al. (1991). This system was included in the rapid variability study carried out by Sokoloski et al. (2001), where a strong detection of flickering was not obtained.

Percy et al. (2001) obtained a power spectrum for EG And and found two periodic variations of periods of 29 and 242 days. The latter variation is approximately half the orbital period; from this, they concluded that EG And is an ellipsoidal variable. Tidal forces distort the surface of the giant component; this varies the stellar surface area observed from the earth and this in turn creates periodic fluctuations in apparent intensity.

Wilson and Vaccaro (1997) treated EG And as an ellipsoidal variable and argued for a low-eccentricity, near circular orbit. However, it was noted that the double-sinusoid lightcurve characteristic of such an effect was not observed in the data acquired in Hric et al. (1991), possibly due to the effect being masked by a major transient event. Wilson and Vaccaro (1997) proposed that if the giant component in EG And was rotating at a rate sub-synchronous to the orbital motion, a dynamical tide would form on the giant's surface. Complicated surface undulations resulting from this tide could provide a mechanism for mass transfer without Roche-lobe filling. They suggested that such a mechanism could cause a transient event that may have masked the ellipsoidal effect, potential explaining the ill-fit of a double sinusoid to the data acquired in by Hric et al. (1991).

Matter transferred through such a mechanism, or indeed any mechanism of accretion onto the hot component, would be subject to ionisation by the hot component's radiation.

Re-emission of this energy is observed in the shorter wavelength region of the optical spectrum. Hence by probing rapid variability in the U and B spectral regions, the nature of the underlying accretion process can be elucidated. In this study, an aim was to quantify the timescales of flickering variability and its causes. This might give some indication as to potential causes of variability, be tidal effects on the giant's surface, disk accretion onto the dwarf or something else.

2.3 Filters and Profiles

Initially, our goal was to collect data at the Johnson B, V, and U filter passbands. The proportional contribution of the hot component and its surroundings is more significant in these spectral regions. Hence, study in these passbands was expected to show variability attributable to processes occurring on or around the hot component. If a symbiotic system is surrounded by a "dusty" nebula, or if the giant has a strong wind, high UV radiation and soft x-rays produced by the WD are reprocessed into higher energy regions of the optical spectrum, Kenyon and Webbink (1984). Data was collected through B and V filters but suitable U-band data was not obtained. The lack of U filter data was resulted of the low apparent magnitude of EG And and its comparison stars in this band, as discussed in chapter 3.1.

Chapter 3

Experimental Method

Poor weather limited us to a handful of observing sessions; therefore only EG And was scrutinised in the execution of the project. A number of older images and data sets relating to EG And were made available.[1]

A set of magnitude and associated error values, taken over the course of 4 years, were obtained from the KAIT telescope in San Jose, California. These magnitudes were used to create phased magnitude plots for EG And.
Ultimately, only one observing session of EG And was carried out at the Monck during the course of the project. Poor weather conditions and problems with the telescope's internal clock and alignment procedures delayed the acquisition of images. Only 21 images were obtained through the B filter and 20 through the V filter, the spectral regions of interest.

3.1 Observations at the Monck Observatory

For our survey at the Monck, the telescope used was a Celestron NexStar 11 GPS-capable Schmidt-Cassegrain Catadiotic with a 279mm Aperture.
The camera used was an SBIG ST-10XME CCD detector. This device had a read noise of $11e^{-1}$rms, a full well capacity of 77,000$e^{-}1$ and a gain factor of 1.31 e^{-}/ADU. The CCD within the camera consisted of a pixel array of dimensions 2184x1472. An on-chip 2x2 binning regime was employed in our survey and therefore all image sequences produced were of dimensions 1092x736.
A telecompressor (TC) was used, providing a wider field of view (FOV); this allowed us to find and identify targets more easily. It is worth noting that for images taken at the Monck, some distortion from circular symmetry was observed in the images of stars. This distortion may have been caused by the inclusion of the TC, although the cause of this distortion wasn't conclusively determined in the study.
The platescales for all of the source telescopes were calculated from the images produced. Previous observers had opted not to make use of a TC at the Monck; the platescale for these observations were determined also. All of the platescales and FOV calculations are included in appendix A.

The filters available at the Monck were made by Custom Scientific and constituted standard UBVR$_c$I$_c$ passbands. Details of their typical central wavelengths and full width at half maxima (FWHM) obtained from Bessell (2005) are tabulated in appendix B.1.
U filter images were not obtained, despite this being a spectral region of particular interest. Three 30 second U-filter test exposures were produced; no comparison stars could be distinguished from the

[1] Images and magnitude data of EG And, obtained at the Imbusch Observatory in Galway, were provided for the project; these weren't used for the final analysis.
Also, new images of another SS, IV Virginis, were obtained at the Watcher telescope in South Africa. These images were of low quality due to pointing and tracking errors and none were used in this study.
The use of the Watcher telescope is ongoing and some requests for corrections were sent to the telescope operators. If another opportunity to observe this system should arise, it may collect data that could be used in future studies.

background and some blurring of the target was present. The lack of comparison stars meant that meaningful magnitude information couldn't be extracted from the images. The blurring error may have been the caused by mechanical error in the telescope's aligning gears or by the apparent motion of the field due to the earth's rotation. In either case, such a blurring effect would worsen with any further increase in exposure time. This prevented us from increasing integration time in order to detect the comparison stars and achieve a sufficient SNR.
Details of further preparations carried out prior to the study are included in appendix C.1.

3.2 Noise Reduction Techniques

Standard image processing and noise reduction techniques were applied to images before aperture photometry was carried out. Images were obtained in the FITS format, allowing the transport of information such as CCD temperature and a timestamp with each image.
For all data obtained at the Monck, image processing and photometry was carried out using a combination of IDL and the astronomical-image processing suites IRIS and Maxim DL. [2]
It was standard practice to cool the CCD to -10^{o}C before images were created to reduce the contribution of temperature-dependant dark current to the data.
For each sequence of raw science frames of a given exposure time, a composite dark frame was created from the median of at least 5 dark frames of the same exposure time. This master-dark was then subtracted from the science frame in order to further minimise the contribution of thermal electrons generated in the CCD array. [3]
Flat frame division was also carried out, as detailed in appendix C.2. A script was written in IDL which normalised a composite flat field to one by dividing the flat field by its median pixel value. Each sequence of dark-subtracted science images was then divided by this normalised flat field.
The overall processing procedure can be written in equation form as

$$\text{final image} = \frac{\text{Raw Science frame - Dark frame}}{(\text{Flat frame - Dark})_{\text{normalised}}}. \tag{3.1}$$

3.3 KAIT Telescope Data

Two data sets obtained with the KAIT telescope were kindly provided by Brian Espey. The KAIT telescope is located at the Lick Observatory, east of San Jose California. It has a 76cm primary mirror diameter and a focal ratio of 8.2. The filters used in this study were Custom Scientific standard UBVR$_c$, the same as used at the Monck. A number of bad lines of data were present in both of these sets, which were removed before further processing. The remaining data was used to form phased differential lightcurves for EG And in U, B, V and R passbands.

Data Set One: EG And and Star A

The first data set consisted of instrumental magnitude values and associated estimates of standard deviation for EG And and a single comparison star. By comparison of the relative magnitudes of the comparison to EG And at each filter, the comparison was identified as HIP 3461, star A in Henden and Munari (2006).
This file consisted of 227 lines of data taken sporadically over the course four years; the earliest magnitude data was taken on 2001.06.20 and the most recent was taken on 2005.01.23.
Treating EG And's orbital period to be 482.57 days, this data set was taken over the course of 2.7 orbital

[2] An initial source of confusion was IRIS's incompatibility with 16bit integers, which is the standard for pixel data in the FITS image format. To ensure compatibility, all pixel values were divided by two before being processed.

[3] Bias offset frames were made when observations were carried out, but they weren't used in the final image processing strategy.; the bias offset is included in dark frames and therefore didn't need to be removed separately.

revolutions of the system.
For each of the U, B, V and R magnitude sequences, both a differential curve and a curve of estimated EG And magnitudes was plotted against the orbital phase of the measurement. These plots are included in the report, see figures 3.1 through 3.8.
The EG And magnitude values were formed by addition of magnitude of star A, as calculated by Henden and Munari (2006), to the instrumental (EG And - star A) magnitude.The introduction of the error associated with the literature magnitudes introduced a significant error to the EG And magnitudes obtained.

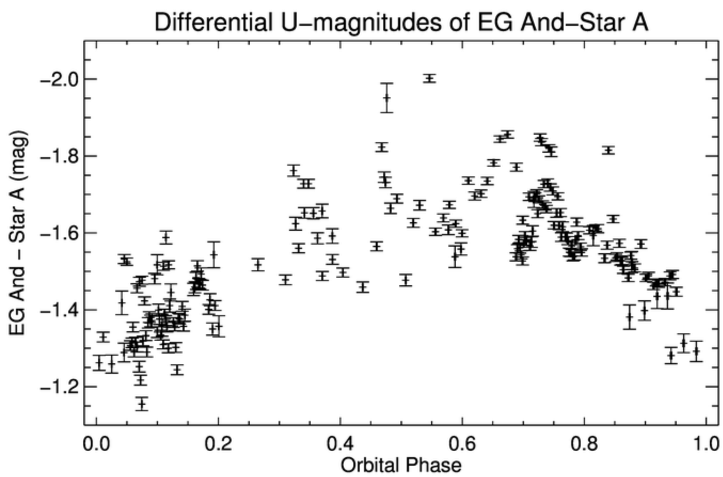

Figure 3.1: KAIT Data Set 1:U filter Differential Curve

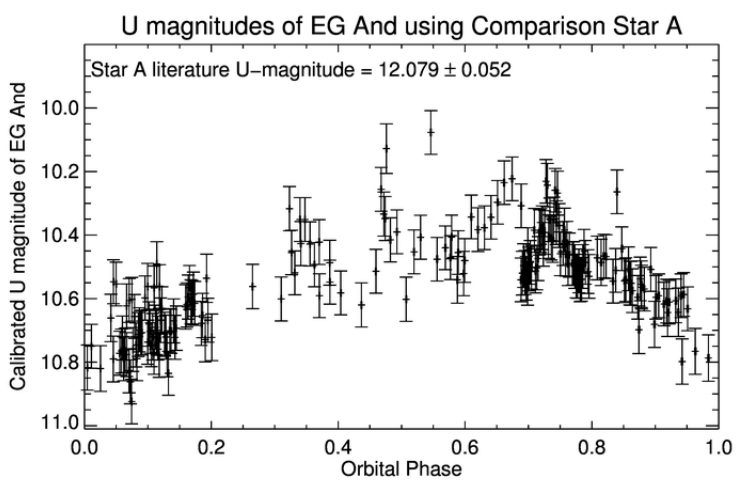

Figure 3.2: KAIT Data Set 1:U filter EG And Curve

Data Set Two: EG And, Star A and Star B

The second data set consisted of magnitude and error data for EG And; HIP 3461 ,star A; and SAO 36621, star B. There were only 29 lines of data in this set as star B was only occasionally in the telescope's FOV.

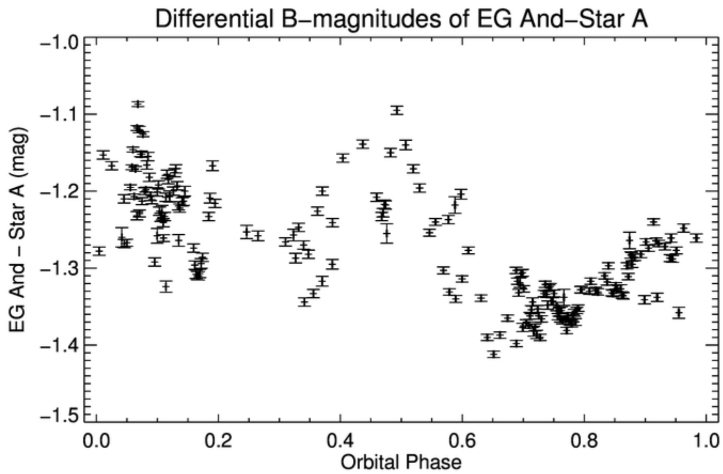

Figure 3.3: KAIT Data Set 1:B filter Differential Curve

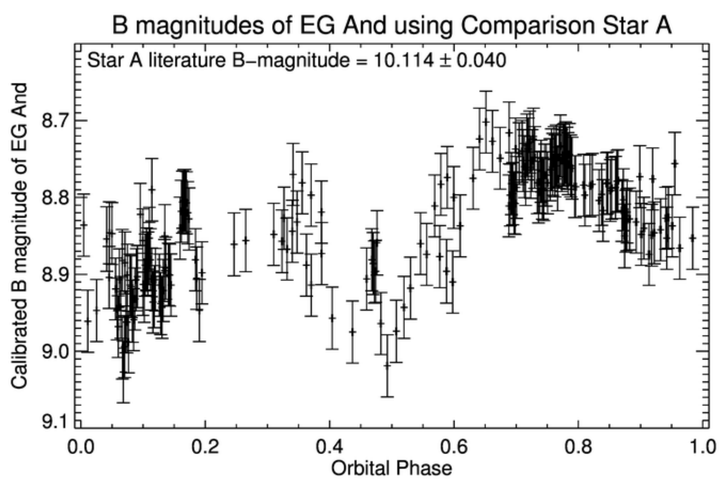

Figure 3.4: KAIT Data Set 1:B filter EG And Curve

A number of these lines contained error values, which were removed before plotting.
Differential curves of (EG And - star A) were plotted alongside differential curves of (star A - star B) for each filter. This allowed us to qualitatively compare the variability observed in the variable source, EG And, with the variability observed in the constant comparison, star A.
These target-and-check magnitude values were plotted over orbital phase to further distinguish the target's inherent variability due to orbital motion from systematic errors that may have been present. The results can be found in figures 3.9 through 3.12.

3.4 Photometric Processing

In order for photometry to be carried out, image sequences had to be aligned and the positions of the stars therein determined. Scintillation, telescope mis-alignment and other effects could cause the position of stars to vary between images.

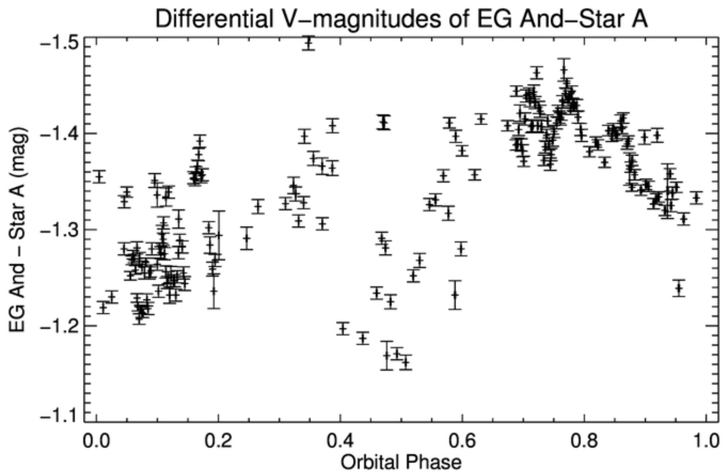

Figure 3.5: KAIT Data Set 1:V filter Differential Curve

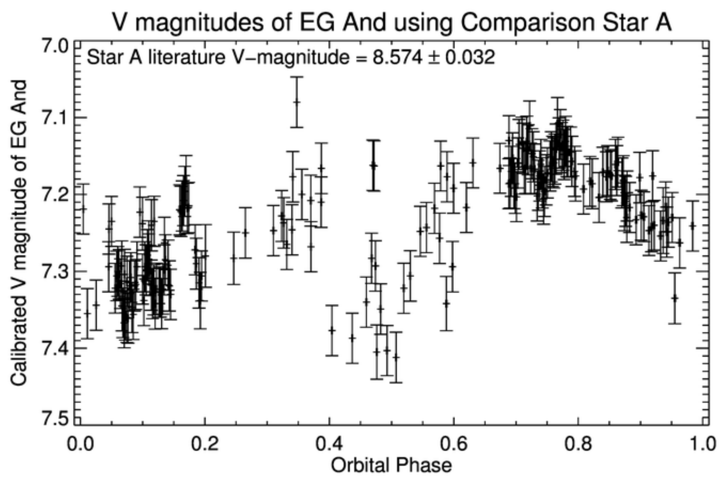

Figure 3.6: KAIT Data Set 1:V filter EG And Curve

To address this, images were aligned in the IRIS software suite. Alignment was carried out by comparison of the pixel position of a single star from image to image; a linear transformation was then applied to each pixel array to align this star from image to image.
This technique could not compensate for more complex changes to the field, such as rotation or other distortions. However, we chose to use it over more mathematically complex transformations because it caused a minimal distortion to the shape of each star's PSF across the pixel array.
Aperture photometry was employed in calculating the incident flux for the target and comparisons. As a general rule, the radius of the aperture was selected to match the FWHM of the PSF of the brightest star under scrutiny. This choice of radius allowed us to acquire a large amount of the total count of each star, while keeping the proportional contribution of the sky background low. A script was written to plot SNR as a function of aperture radius. Ultimately, the brightest star's FWHM was used to determine the extraction for all image sequences, as it consistently provided a high SNR.
We replicated the estimations of uncertainty in photometric measurements outlined by Sokoloski et al. (2001) for our own study. An abbreviated description of this uncertainty estimation is provided below.

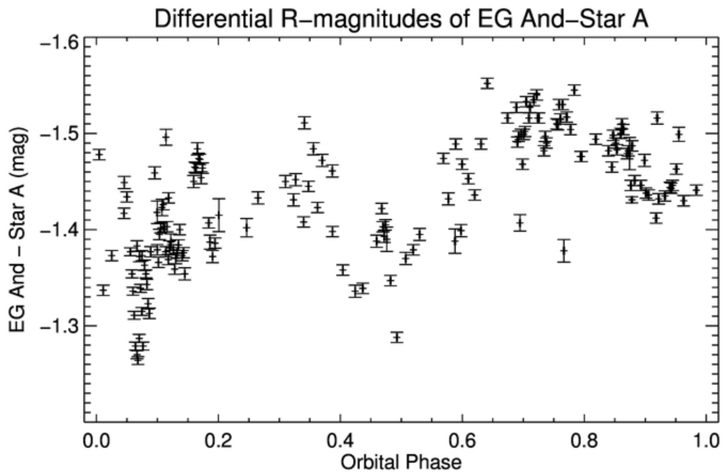

Figure 3.7: KAIT Data Set 1:R filter Differential Curve

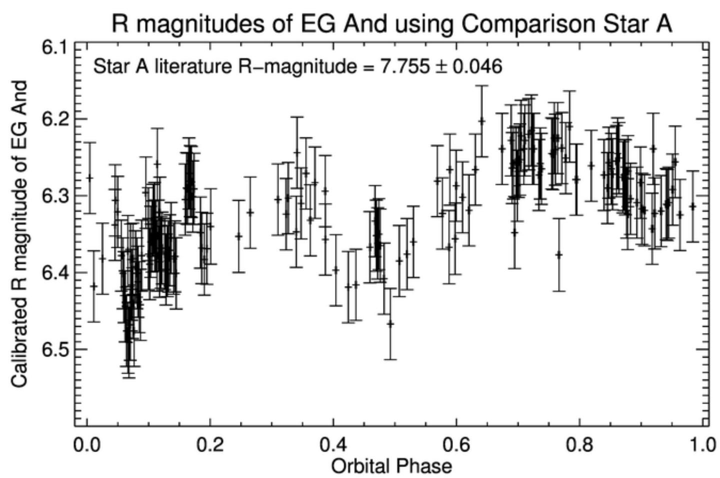

Figure 3.8: KAIT Data Set 1:R filter EG And Curve

An estimation of the variance when CCD aperture photometry is applied to a star is given by the CCD equation, equation Howell (1992);

$$\sigma^2_{CCD} = c + n_{bins}\left(1 + \frac{n_{bins}}{n_{sky}}\right)(N_S + N_R^2 + N_D)); \tag{3.2}$$

c is the integrated stellar count in electrons,n_{bins} is the area of the software aperture in bins; n_{sky} is the number of area of region used for background estimation in bins;N_S is the sky (background) counts, in electrons per bin; N_R is the read noise, in rms electrons per bin; and N_D is the dark current, in electrons per bin.

To account for the variations introduced by atmospheric scintillation, we adopted Young's formulation Young (1967) of Reiger's theory of scintillation Reiger (1963);

$$s_{scint} = \frac{c_{rms}}{\bar{c}} = S_0 d^{-2/3} X^{3/2} e^{-h/h_0} \Delta f^{1/2}, \tag{3.3}$$

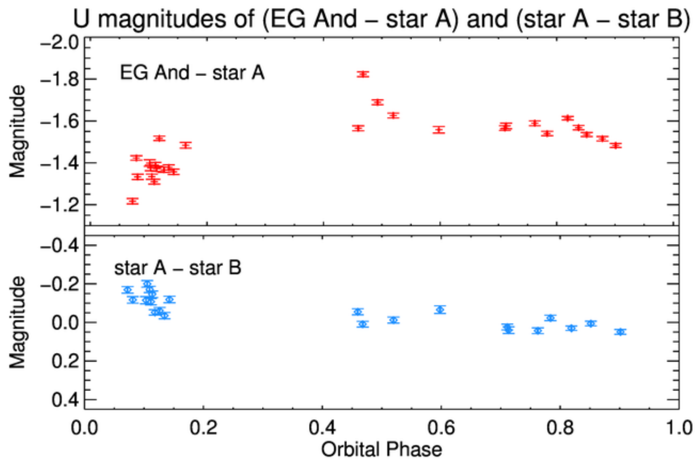

Figure 3.9: KAIT Data set 2:U Filter plot of (EG And -star A) and (star A - star B)

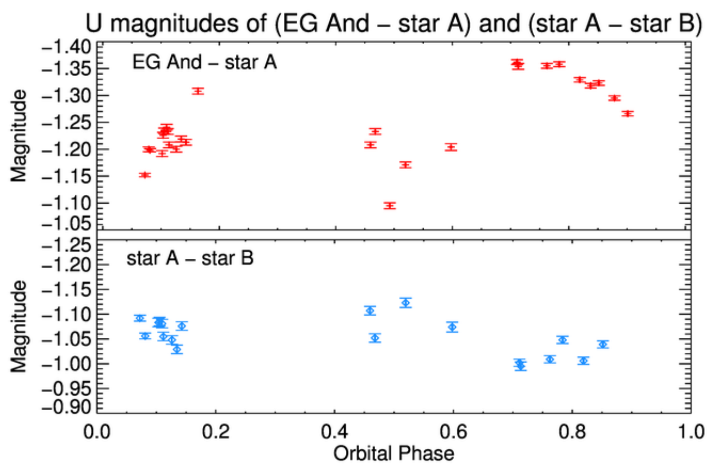

Figure 3.10: KAIT Data set 2:B Filter plot of (EG And -star A) and (star A - star B)

where s_{scint} is the percentage rms variation due to scintillation, $\bar{c}$ is the mean value of c from a series of measurements, S_0 is a constant that Young (1967) found from observations to be 0.09, d is the mirror diameter in cm, X is the air mass, h is the observatory altitude im meters, $h_0 = 8000$ m, and Δf is the frequency bandpass of time-series sampling rate in Hz, i.e. $= 1/t_{int}$, where t_{int} is the integration time in seconds.
The expression for the total expected variance for each star is thus

$$\sigma_m^2 = \sigma_{CCD,m}^2 + s_{scint}^2 c_m^2, \tag{3.4}$$

where $\sigma_{CCD,m}$ is σ_{CCD} for star m.

3.5 Light Curve Formation

Two techniques were considered and applied to form light-curves for the target star from our images. Differential photometry with one comparison star was considered as it required the inclusion of fewer

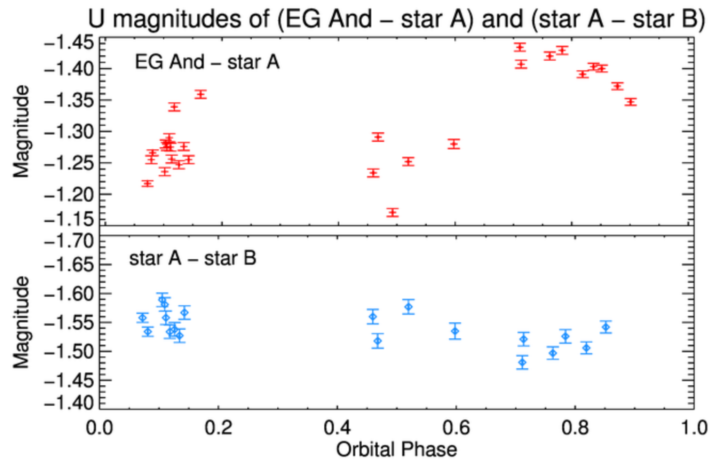

Figure 3.11: KAIT Data set 2:V Filter plot of (EG And -star A) and (star A - star B)

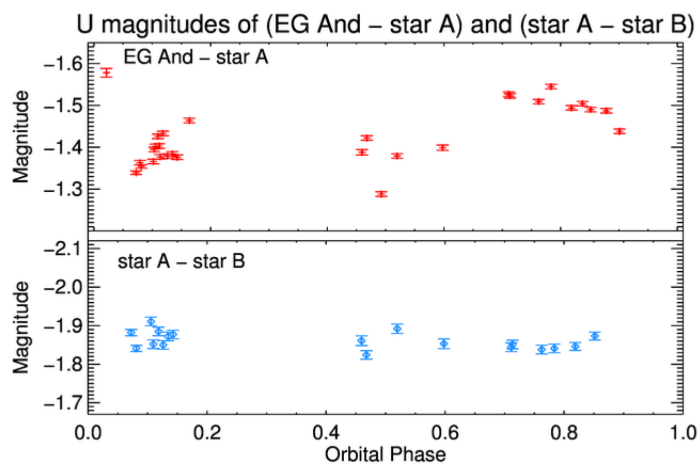

Figure 3.12: KAIT Data set 2:R Filter plot of (EG And -star A) and (star A - star B)

comparison stars in the field; also, it is more computationally straightforward to carry out. Differential photometry with an ensemble of comparison stars was had appeal as this technique promised a higher sensitivity to periodic and aperiodic variability. Both techniques were employed and some sensitivities obtained are tabulated in table 4.1.

Typical images of EG And had four suitable comparison stars whose magnitudes and locations were known from Henden and Munari (2001). These nearby stars of stable magnitude allowed us to carry out the differential-ensemble technique employed by Sokoloski et al. (2001). This technique reduced uncertainty in our final light curve data points and enabled us to probe to smaller magnitudes of variability than would otherwise have been achievable.

Differential Photometry with a Single Comparison

The magnitude difference between the target and a single comparison star was plotted for the B, V and R filter data obtained at the Monck. The differential Curve of the comparison star and a check star was plotted alongside this.
The results are presented in figures 3.13 through 3.15.

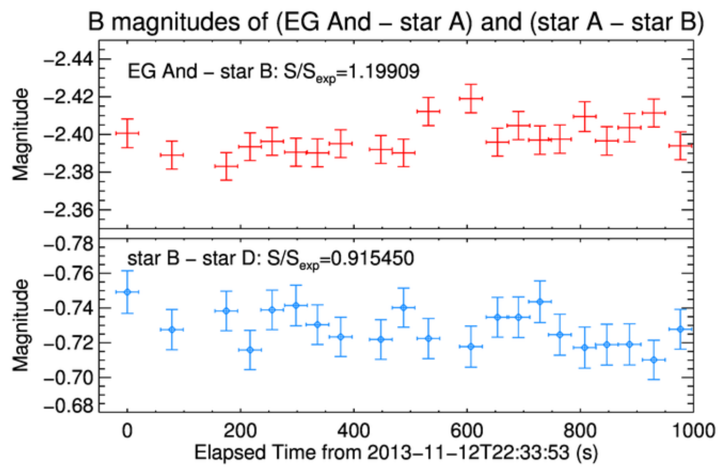

Figure 3.13: Differential B magnitudes of EG And, a comparison and a check star

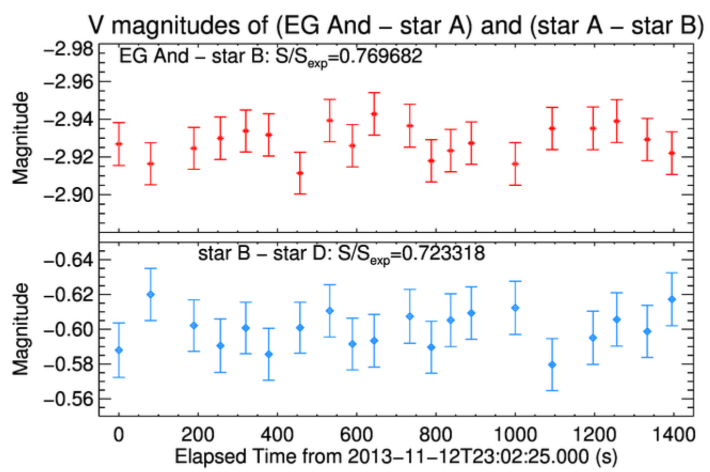

Figure 3.14: Differential V magnitudes of EG And, a comparison and a check star

Differential Photometry with Weighted-Mean Ensemble

A method of forming a lightcurve of weighted-mean, normalised count ratio values using an ensemble of comparison stars was adopted from Sokoloski et al. (2001). This method was in turn an application of the weighing scheme introduced by Gilliland and Brown (1988).

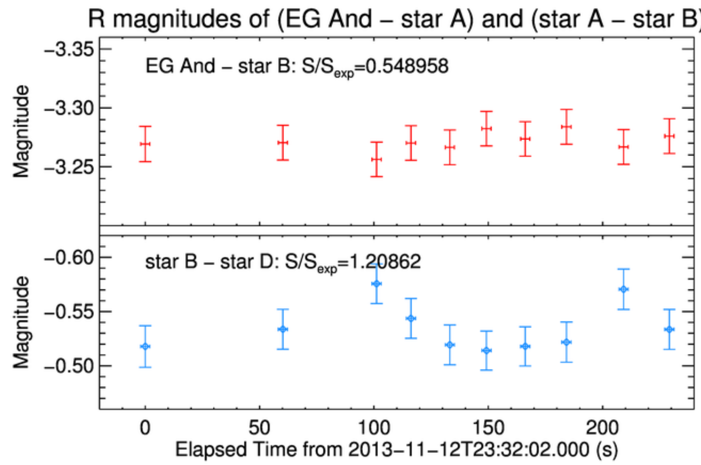

Figure 3.15: Differential R magnitudes of EG And, a comparison and a check star (2 second exposures)

Note that the curves produced by this technique are not magnitude values; the curve is a measure of the deviation of the flux. The flux is normalised to unity and a change of +0.001 corresponds closely to a change of +1 mmag.
For each image in a sequence of N images a script was written in IDL which calculated the ratio of the programme star counts to a weighted-sum of comparison star counts;

$$x(i) = A\frac{C_p(i)}{\sum_{m=1}^{K} w_m C_m(i)}.i = 0, ...N-1, \tag{3.5}$$

$x(i)$ is the count ratio for the ith image; $C_p(i)$ is the background-subtracted source counts for the programme star in the ith image; $C_m(i)$ is the background-subtracted source counts for comparison star m in the ith image; w_m is the statistical weight for the mth comparison star, which is the same across all images, i; and K is the number of comparison stars used.
A is the normalisation factor; this is given by

$$A^{-1} = \frac{1}{N}\sum_{j=0}^{N-1}\frac{C_p(j)}{\sum_{n=1}^{K} w_n C_n(j)}. \tag{3.6}$$

For the mth comparison star, the statistical weight is given by

$$w_m = \frac{\overline{C_m}}{\overline{\sigma_m^2}} = \frac{\sum_{i=0}^{N-1} C_m(i)}{\sum_{i=0}^{N-1} \sigma_m^2(i)}. \tag{3.7}$$

σ_m is the formal uncertainty on the mth comparison; $\overline{C_m}$ and $\overline{\sigma_m}$ are the averages over all N images of C_m and σ_m, respectively.

Chapter 4

Results and Analysis

The differential-ensemble technique discussed in section 3.5 was applied to the B, V and R data sets obtained at the Monck Observatory on 2013.11.13. The lightcurves produced are plotted in figures 4.1 and 4.3.
The error bars in the plots were obtained from the standard deviation as calculated from the propagation of the uncertainties associated with the program star and the comparisons used to form the ensemble set. The calculation of the variance and the standard deviation for each point in the light curve is discussed in section 4.1.

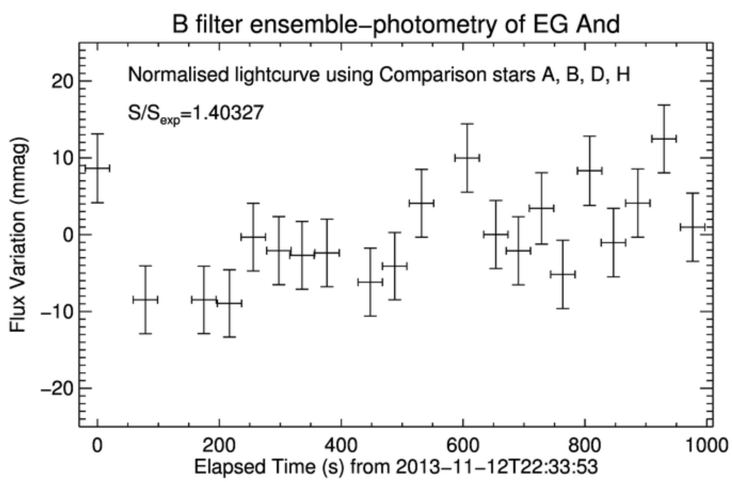

Figure 4.1: EG And B-filter Normalised Lightcurve

4.1 Error and Uncertainty

Error in Single-Comparison Differential Photometry

The formal error associated with the difference between two magnitude values, m_1 and m_2, as calculated from their respective photon counts, is given by

$$\sigma^2_{m_1-m_2} = \left(\frac{2.5}{ln(10)}\right)^2 \left(\frac{\sigma_1^2}{c_1^2} + \frac{\sigma_2^2}{c_2^2}\right). \tag{4.1}$$

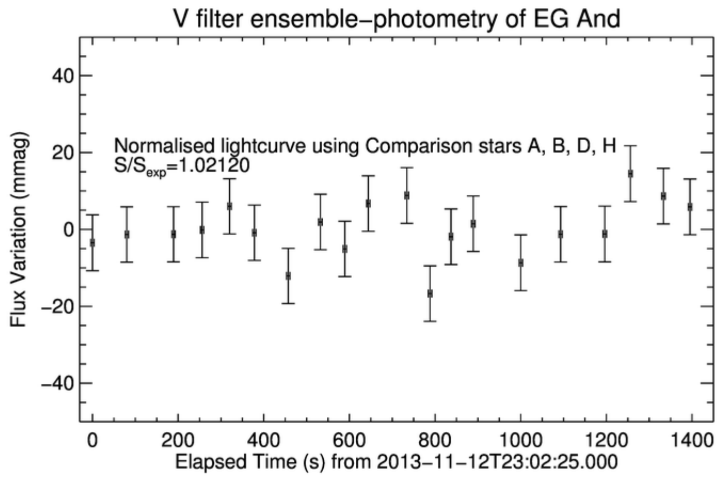

Figure 4.2: EG And V-filter Normalised Lightcurve

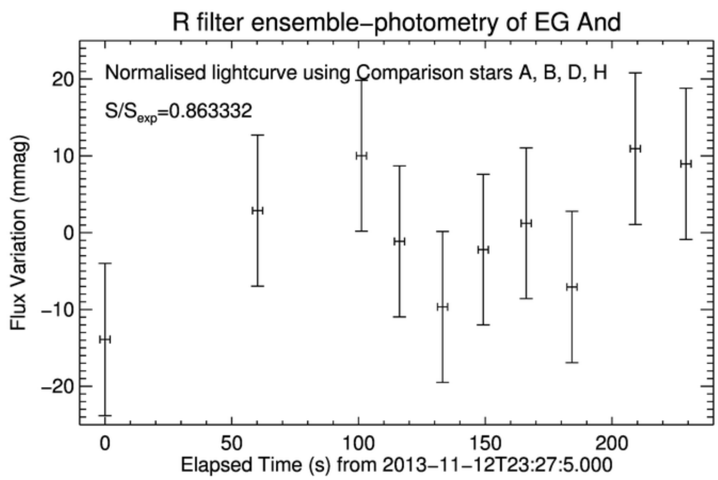

Figure 4.3: EG And R-filter Normalised Lightcurve

c_1 and c_2 are the counts from object 1 and object 2; σ_1 and σ_2 are the standards deviations associated with object 1 and 2.

Error in Weighted-Mean Ensemble Calculations

The expected variance for a data point $x(i)$ is calculated via the weighted-mean technique is given by the relation

$$\sigma_x^2(i) \approx \left[\frac{\sigma_x(i)}{x(i)}\right]^2 = \left[\frac{\sigma_p(i)}{c_p(i)}\right]^2 + \frac{\sum_{m=1}^{K}[w_m \sigma_m(i)]^2}{[\sum_{n=1}^{K} w_n C_n(i)]^2}, \tag{4.2}$$

where $\sigma_x^2(i)$ is the expected variance for the data point $x(i)$. Note that because the x values are normalised to unity, the variance values calculated from the above equation are approximately equal to their corresponding fractional variances, as highlighted in the equation above.
The weighted average of the expected variance over all the points in the light curve, S^2_{exp}, was calculated

Table 4.1: Average expected RMS variations and S/S_{exp} values

Stars used	Filter	Exposure time (s)	$\overline{s_{exp}}(mmag)$	$\frac{S}{S_{exp}}$
Lightcurves Obtained with Single Comparison				
EG And/star B	B	20s	5.77	1.99
EG And/star B	V	4s	9.09	0.77
EG And/star B	R	2s	12.6	0.55
star B/star D	B	20s	11.6	0.92
star B/star D	V	4s	15.11	0.72
star B/star D	R	2s	18.40	1.21
Lightcurves Obtained with a Weighted-Mean Ensemble				
EG And/stars A,B,D,H	B	20s	4.44	1.4
EG And/stars A,B,D,H	V	4s	7.21	1.02
EG And/stars A,B,D,H	R	2s	9.84	0.86
EG And/stars D,H	B	20s	9.06	1.06
star B/stars D,H	B	20s	10.58	0.91

for each set of images.

$$S_{exp}^2 = \frac{\sum_{i=0}^{N-1}\left[\frac{1}{\sigma_x^2(i)}\sigma_x^2(i)\right]}{\sum_{i=0}^{N-1}\frac{1}{\sigma_x^2(i)}} = \frac{N}{\sum_{i=0}^{N-1}\frac{1}{\sigma_x^2(i)}} \tag{4.3}$$

This parameter was combined with the observed variance in the data set in the search for flickering variability.
Sokoloski et al. (2001) utilised the ratio of the observed variance of the lightcurve to the variance expected from known errors as a diagnostic for the presence of flickering in the target.
The observed variance for a series of N data points, where the error on each point is different is given in equation 4.4, which is discussed in (Robinson, 1992, pp. 195).

$$s^2 = \frac{N}{N-1}\frac{\sum_{i=0}^{N-1}\left(\frac{x_i-\overline{x}}{\sigma_i}\right)^2}{\sum_{j=0}^{N-1}\frac{1}{\sigma_j^2}} \tag{4.4}$$

$\frac{S}{S_{exp}}$ ratios calculated for a number of the differential techniques are tabulated in table 4.1.

For a ratio $\frac{S}{S_{exp}} \approx 1$, the target's signal is a good match to that of a star of constant flux without variation.
As this ratio increases, the likelihood of variations being the result of an inherent variability target increases also. By reducing the noise and uncertainty from known sources as much as possible, one can minimise the expected uncertainty across the whole lightcurve; thus allowing the S/S_{exp} parameter to be sensitive to the smallest magnitude of flickering achievable.
For this reason it is very important that the contribution of various noise sources is reduced as much as possible in order to increase our sensitivity to flickering.
For a number of both the single-comparison and ensemble-curves, this ratio was found to be less that one. This result indicates an over-estimation of the expected variance of the signal.
Attempts were made to determine the cause of this over-estimation; it could be contributed to a number of factors.
In all calculations of uncertainty, the $(N_s+N_r^2+N_d)$ term in the CCD equation, equation 3.2, was replaced by the measured variance of pixels used to estimate the sky background noise. This measured variance value was consistently greater than or equal to the documented contributions to variance from the read noise, dark noise and sky background noise. Hence this substitution resulted in a very conservative calculation of uncertainty.
Another systematic error was introduced through this method which erroneously increased our estimates

of uncertainty. A star lay in the annulus surrounding comparison star A, which consistently increased the standard deviation in sky background calculations. The same radii were used for all target areas and surrounding annuli for all stars used in photometry for a given filter sequence and therefore, the annulus around star A couldn't have been changed without potentially introducing problems from other star annuli.
In their efforts to further evaluate a detection of short-timescale flickering variability in EG And, Sokoloski et al. (2001) carried out ensemble photometry on a bright comparison star in the field and compared the results to a lightcurve produced by differential photometry of EG And using the same comparison stars. This had been employed in order to expose potential systematic errors that had not been eradicated in image pre-processing or through the differential photometry.
In an attempt to determine the source of the variance over-estimation observed in our data, a similar comparison of differential curves was performed, see figures 4.4) and figure 4.5.

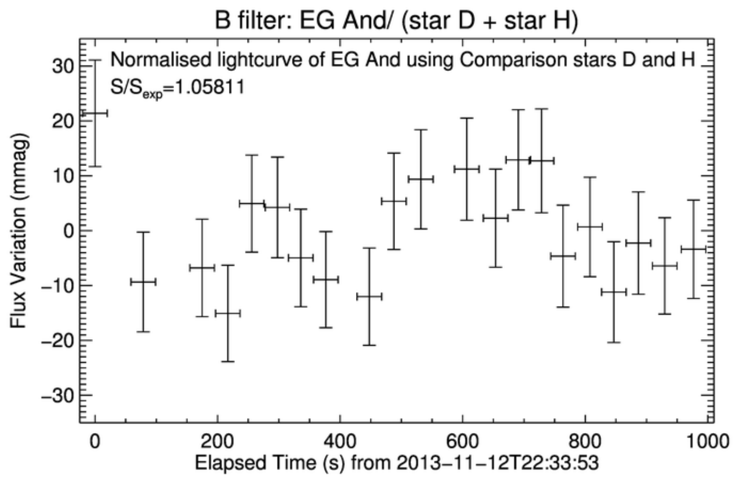

Figure 4.4: B filter Normalised Lightcurve of EG And/(D + H)

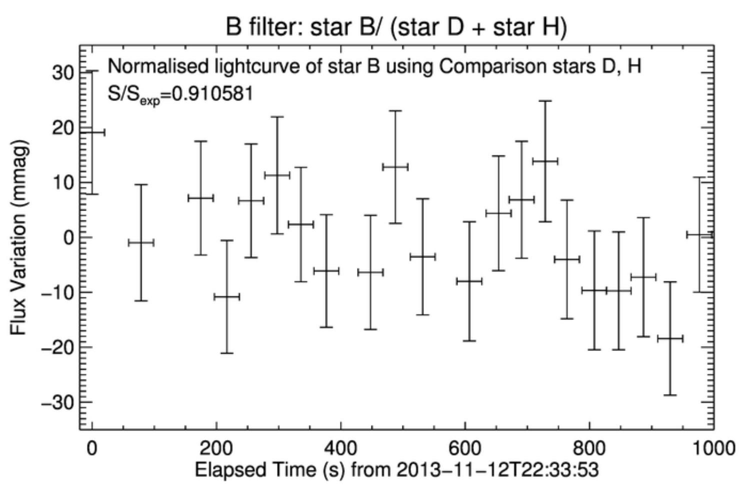

Figure 4.5: B filter Normalised Lightcurve of B/(D + H)

Differential lightcurves were combined with magnitude data from the KAIT telescope in the formation of B and V differential magnitudes.These are included in figures 4.6 and 4.7.

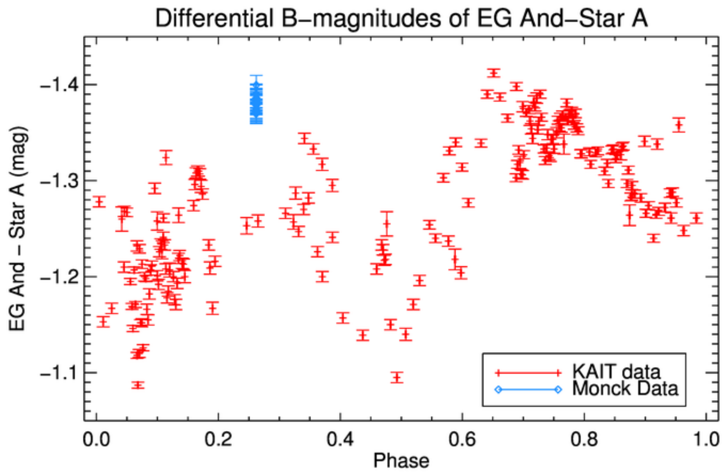

Figure 4.6: B filter: Phased KAIT and Monck Data

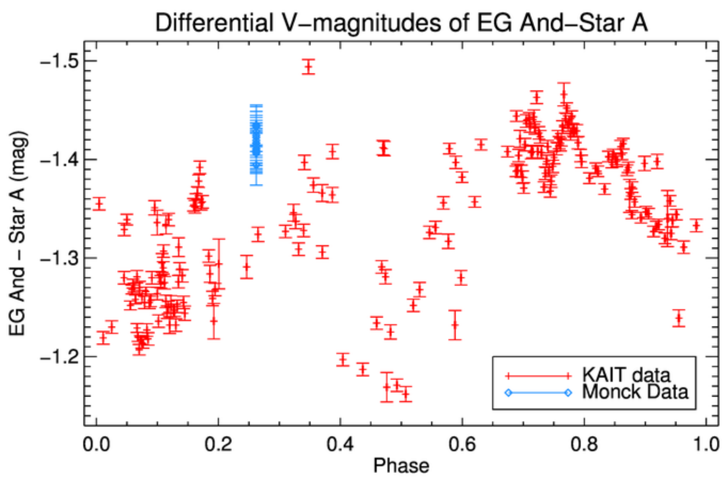

Figure 4.7: V filter: Phased KAIT and Monck Data

Chapter 5

Discussion and Conclusions

The ensemble differential photometry plot of star B, figure 4.5, with a plot of EG And using the same comparison stars, figure 4.4, yielded similar values of s_{exp} and s/s_{exp}. This could be taken as an implication of a stable flux for EG And at these magnitudes. This data set was small and is therefore of little significance statistically. At the very least, a null result such as this warrants a larger data set for variability at these magnitudes to be ruled out.
The ratio of the observed fractional variance to the fractional variance expected from known errors was the parameter used in our search for very short timescale aperiodic variability in EG And.
The highest sensitivity was achieved with differential ensemble photometry, as outlined in section 3.5.
In their search for flickering variability, Sokoloski et al. (2001) found some indication of flickering variability for EG And.
Were we to choose a value of $s/s_{exp} \geq 2$ as an indicator for flickering detection, the magnitudes of flickering to which we be sensitivity can be estimated. For the differential-ensemble lightcurve produced by our sequence of 20 second B exposures, we calculated the average expected standard deviation to be 4.4 mmag.
We are therefore sensitive to flickering of the order of 8.8 mmag occurring at timescales $\geq$ 20 seconds.
Using the same criteria of $s/s_{exp} \geq 2$ as a detection of flickering, we can claim sensitivity to flickering in the V passband of the order 14.42 mmag at timescales $\geq$ 4 seconds.
Note that although these estimates of sensitivity does not imply detections or non-detections in the data sets obtained. They small number of images obtained severely limits the statistical significance of calculations carried out.

Appendix A

Platescale Calculations

The plate scale (PS) was calculated for a number of telescope fields. For a given field and telescope, the known difference in right ascension(RA) and declination(Dec) of two stars was compared with their pixel separation in the field. The RA, Dec and associated error values for stars in the Watcher telescope images of IV Virginis were obtained from Henden and Munari (2001). For comparison stars in EG And's field, the RA and Dec values were obtained from Henden and Munari (2006).For an image taken through each telescope, the PS was calculated according to the following equation;

$$PS = \frac{\sqrt{(RA_2 - RA_1)^2 + (Dec_2 - Dec_1)^2}}{\sqrt{(X_2 - X_1)^2 + (Y_2 - Y_1)^2}} \text{degrees pixel}^{-1}$$

, where (X_1, Y_1) and (RA_1, Dec_1) are star one's pixel and RA/Dec locations, respectively. (X_2, Y_2) and (RA_2, Dec_2) are star two's pixel and RA/Dec locations, respectively.
This equation takes RA and Dec to be both given in degrees.
Using this method, the platescale and sidelengths of images taken at the Monck Observatory, the Imbusch Observatory and the Watcher telescope were calculated. The results are tabulated in table A.1.

Watcher Telescope

The stars used to calculate the plate scale for the Watcher telescope were IV Virginis and its closest comparison star.

Imbusch and Monck Observatories

The platescale of images obtained from the Imbusch and Monck observatories were calculated from the separation of the two closest comparison stars to EG And, comparison stars A and B in Henden and Munari (2006).

Table A.1: Platescale Calculations for Data Sources.

Instrument	PS(")	△ PS (")	X sidelength (')	Y sidelength(')
Watcher	0.486	0.0043	8.29	8.29
Monck(TC)	1.668	0.008	30.47	20.46
Monck(no TC)	1.277	0.005	23.32	15.66
Imbusch	0.988	0.003	16.86	16.86

Appendix B

Filter Passbands

Filter passband FWHM values and central wavelengths for UBVR$_c$I$_c$ filters, as given in Bessell (2005), are tabulated below.

The filters in use at the Monck and KAIT telescopes were both Custom Scientific filters covering the UBVR$_c$I$_c$ passbands. A convenient image of these bands was obtained from the SBIG website, see figure B.1.

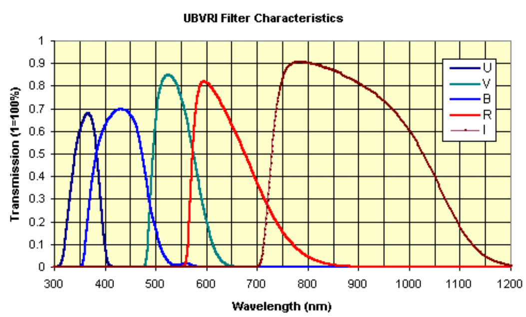

Figure B.1: Custom Scientific Filter Passbands

Table B.1: Central Wavelengths and FWHM in $\mathring{A}$

UBVRI		
Filter	λeff	$\Delta\lambda$
U	3663	650
B	4361	890
V	5448	840
R	6407	1580
I	7980	1540

Appendix C

Preparations at the Monck Observatory

C.1 Prior to the Study

The ST-10XME Camera uses a desiccant to lower the internal dew point to temperatures below the operating temperature of the CCD. This prevents the formation of frost when the CCD's thermoelectric cooler is employed to reduce dark current. In preparation for our survey, the camera's desiccant was regenerated overnight at $\sim$175°C in a laboratory oven.
An observing session was dedicated to ensuring that the azimuthal mount was aligned correctly and that the telescope was properly collimated. A drift alignment procedure was carried out to ensure that the azimuthal mount was polar aligned; when a star was centred using a cross-hair eyepiece, it wouldn't drift significantly from the centre of the field after 10 minutes.
Collimation was carried out to ensure that the telescopes internal optics were correctly aligned and centred.

C.2 Flat Fields

In order to obtain flat-fields, the light of a halogen lamp was passed through a white cloth and onto a flat, white board on the wall of the observatory's dome. The source was arranged to be suitably uniform and featureless such that any structure or distortion observed in the images was solely the result of the dust or imperfections in the telescopes optical train. The exposure time for each filter's flat frame was such that the median value in the image was approximately a third of the saturation point of the detector, in the region of 19,000 ADU.
For the 2013 observation session, master flats were created for each filter by median combination of 5 dark-subtracted flat images. Note that the darks used were in turn median composite master-darks of the same exposure time and temperature as the flat field image.

Bibliography

Bessell, M. S. (2005). Standard Photometric Systems. , 43:293–336.

Fekel, F. C., Joyce, R. R., Hinkle, K. H., and Skrutskie, M. F. (2000). Infrared Spectroscopy of Symbiotic Stars. I. Orbits for Well-Known S-Type Systems. , 119:1375–1388.

Gilliland, R. L. and Brown, T. M. (1988). Time-resolved CCD photometry of an ensemble of stars. , 100:754–765.

Henden, A. and Munari, U. (2001). UBV(RI)$_C$ photometric comparison sequences for symbiotic stars. II. , 372:145–151.

Henden, A. and Munari, U. (2006). UBV(RI)C photometric sequences for symbiotic stars. III. , 458:339–340.

Howell, S. B., editor (1992). *Astronomical CCD observing and reduction techniques*, volume 23 of *Astronomical Society of the Pacific Conference Series*.

Hric, L., Skopal, A., Urban, Z., Dapergolas, A., Hanžl, D., Isles, J. E., Niarchos, P., Papoušek, J., Pigulski, A., and Velić, Z. (1991). Photometry of symbiotic stars - an international campaign. II. Z And, EG And, R Aqr, UV Aur, TX CVn, T CrB, BF Cyg, CH Cyg, CI Cyg, V1016 Cyg, V1329 Cyg, AG Dra, CQ Dra (4 Dra), NQ Gem, YY Her, V443 Her, RW Hya, SS Lep, BX Mon, RS Oph, Hen 1341 Oph, AG Peg, AX Per, HM Sge, QW Sge (AS 360), FR Sct (AS 296), AS 289 Ser, PU Vul. *Contributions of the Astronomical Observatory Skalnate Pleso*, 21:303–331.

Kenyon, S. J. (1986). *The symbiotic stars.*

Kenyon, S. J. and Webbink, R. F. (1984). The nature of symbiotic stars. , 279:252–283.

Percy, J. R., Wilson, J. B., and Henry, G. W. (2001). Long-Term VRI Photometry of Small-Amplitude Red Variables. I. Light Curves and Periods. , 113:983–996.

Reiger, S., H. (1963). , 68:395.

Robinson, P. R. B. D. K. (1992). *Data reduction and error analysis for the physical sciences.* McGraw-Hill, 3rd ed edition.

Skopal, A., Chochol, D., Vittone, A. A., Blanco, C., and Mammano, A. (1991). Spectroscopic and photometric studies of the symbiotic star EG Andromedae. , 245:531–542.

Sokoloski, J. L., Bildsten, L., and Ho, W. C. G. (2001). A search for rapid photometric variability in symbiotic binaries. , 326:553–577.

Wilson, R. E. and Vaccaro, T. R. (1997). Ellipsoidal variation in EG Andromedae. , 291:54–58.

Young, A. T. (1967). Photometric error analysis. VI. Confirmation of Reiger's theory of scintillation. , 72:747.